www.czasopisma.pan.pl PAN POLSKA AKADEMIA NAUK www.journals.pan.pl

Archives of Acoustics Vol. **48**, No. 3, pp. 433–449 (2023), doi: 10.24425/aoa.2023.145238

Research Paper

A Microscopic Prediction Model for Traffic Noise in Adjacent Regions to Arterial Roads

Ming LI[(1)], Jizhou LIU[(2)]*

[(1)] *School of Transportation Engineering, Shandong Jianzhu University*
Jinan, China

[(2)] *School of Thermal Engineering, Shandong Jianzhu University*
Jinan, China

*Corresponding Author e-mail: liujizhou20@sdjzu.edu.cn

(*received October 7, 2022; accepted December 30, 2022*)

Traffic noise in big cities impacts the people who live and work in high-rise buildings alongside arterial roads. To determine this impact magnitude, this paper proposes and validates a microscopic level method that locally predicts the total noise level and the spectral characteristics of traffic flow in the near-road region. In the proposed method, the vehicles on the road are considered as multiple queues of moving point sound sources with ground reflection considered. To account for the flow of vehicles on the road, traffic field data, and individual vehicle noise source models are also employed. A field measurement is conducted to validate the proposed method. Results comparison shows that the predicted and the measured overall A-weighted sound pressure level and A-weighted noise spectra are within 3 dBA and 5 dBA, respectively. Based on the validated method, the spatial distribution of traffic noise near the arterial road is investigated for different traffic scenarios.

Keywords: traffic noise; arterial roads; noise prediction method; microscopic level.

1. Introduction

1.1. Background and motivations

In many big cities, arterial roads, and overhead freeways have been constructed in the urban areas or between the urban and suburban areas to meet the cities' transportation demands. Due to the high traffic speed and volume, the noise generated by traffic flows on such roads is much more important than that generated by traffic on secondary streets. In many densely populated cities, it is common for high-rise buildings, whether residential, educational, business or commercial, to be built just by the overhead freeways or no more than several hundred meters away from the arterial roads. People who live or work in those buildings experience daily traffic noise annoyance, which can be harmful to their health (Lokhande *et al.*, 2018; Barrigón Morillas *et al.*, 2022; Sanok *et al.*, 2022).

To evaluate the traffic noise impact on existing or planned infrastructures, a series of traffic noise prediction methodologies have been established. Depending on the scope and degree of detail of the researched problem, these methods could be divided into three categories. The first methodology is the deterministic model. It relies on single vehicle noise emission model as well as traffic speed and volume data (Nielsen *et al.*, 1996; Bendtsen, 1999; Kephalopoulos *et al.*, 2012; Directive EN, 2015; Lin *et al.*, 2012; Peng *et al.*, 2019). Although the prediction range is limited, detailed information, such as the third-octave spectra and higher accuracy, is ensured. The second modeling category, based on the noise map (Hinton *et al.*, 2005; Popp, 2003), extends the road traffic noise prediction to city regions (Lee *et al.*, 2008). By noise maps, the traffic noise exposure of the population could be estimated (Kaddoura *et al.*, 2017; Lan *et al.*, 2020; Lokhande *et al.*, 2017). However, for regional or even

national scale noise exposure estimation, incomplete data makes the noise map partially efficient. For such a scale, the statistical model (Staab *et al.*, 2022) based on available data and linear land-use regression could be employed.

In view of the traffic noise issue alongside arterial roads in big cities, this paper targets to develop a traffic noise prediction method at a microscopic level, which is applicable to evaluating locally the impact of traffic noise from a segment of the arterial road on people living or working in nearby high rise buildings, and provides detailed spectral features and noise level spatial distributions. Under such circumstances, the width of the noise source could vary from 25 m to over 60 m depending on the road width, while the distance of the observer in nearby buildings from the road is mostly no more than 500 m, making the dimension of the noise source non-negligible as compared to the range of sound propagation.

The method proposed by this paper aims at predicting locally the traffic noise near a segment of big roads with the multi-lane configuration of the arterial road considered to avoid the linear source assumption (Steele, 2001; Quartieri *et al.*, 2009). On each lane, the vehicles are modeled as a queue of moving point sound sources in half space. The time-dependent sound pressure field of each vehicle is derived by acoustic theory considering the translational movement of the vehicle and the reflection of the ground. At the receiver point, the total sound pressure at a certain moment is considered as the superposition of the sound pressure fields of all the vehicles on the road. The noise intensity of each vehicle as a point source follows the noise emission expression in (Lin *et al.*, 2012) and the noise spectral characteristics for different vehicle types follow the work of Yang *et al.* (2020). The sound attenuation effect of trees by the road is also considered. Therefore, the valid range of the method is in the vicinity of arterial roads where the road width makes simple line source assumption less suitable. The 1/3 octave sound pressure level spectra could be predicted with different lane configurations, vehicle speeds, and vehicle types.

1.2. Related work

In predicting traffic noise alongside roads, three basic elements are needed: 1) the noise source characteristics: the noise level and spectral characteristics of a single vehicle depending on vehicle speed and type; 2) traffic flow data: including traffic speed data and traffic volume data; 3) the propagation module: the noise emission model that estimates the noise intensity at a certain distance away from the vehicle. Many researchers worked on these elements and have laid a well-established foundation for reference.

To obtain the noise source characteristics of a single vehicle, field tests have been conducted with different vehicle types, speeds, accelerations, and road surface status. By collecting noise measurement results near the roads in the Nordic countries, the Nordic Prediction method (Nielsen *et al.*, 1996; Bendtsen, 1999) established the noise emission curves as a function of vehicle speed for light and heavy vehicles. Lin *et al.* (2012) measured the noise data of light, medium. and heavy vehicles at a traffic intersection and established the relationship of the sound pressure level of a single vehicle as a function of speed and acceleration at a reference location of 7.5 m from the first lane. In the report of Common Noise Assessment Methods in Europe (CNOSSOS-EU) (Kephalopoulos *et al.*, 2012; Directive EN, 2015), the influence of frequency and noise source type was introduced to the source emission module. For instance, the vehicle noise is decomposed into rolling noise and propulsion noise. Their dependencies on vehicle speed and frequency were provided, respectively. To obtain detailed spectral noise characteristics, Luo *et al.* (2013) and Yang *et al.* (2020) collected and classified the 1/3 octave noise spectral energy contribution of single vehicles based on vehicle type and speed, which allows the prediction of the traffic noise spectrum.

Another aspect of traffic noise prediction is to relate the noise emitted by the traffic flow with the receiver at a certain point. A variety of models have been established by researchers from different countries. For example, see the FHWA (Barry, Reagan, 1978), the CoRTN (CoRTN, 1975), the RLS 90 (RLS, 1990), the Nord2000 (Nielsen *et al.*, 1996; Bendtsen, 1999), the NMPB-Route-2008 (Dutilleux *et al.*, 2010), and the CNOSSOS-EU (Kephalopoulos *et al.*, 2012; Directive EN, 2015; Khan *et al.*, 2021). In these models, the propagation module adopts the energy type equation or the ray tracing theory to calculate the sound attenuation caused by geometrical divergence during the propagation. Influences of the absorption of air, the effect of obstacles, the reflection of the ground, etc., are also implemented in the models. By using these emission models, the equivalent sound pressure level of traffic flow could be estimated. For instance, Stoilova and Stoilov (1998) applied this kind of model to study noise pollution control by traffic lights. In (Yang *et al.*, 2020) the noise spectrum of the traffic flow was calculated based on a localized noise emission model.

2. Methodology

This section describes the formulation of the proposed method from a single vehicle to the traffic flow on the road.

2.1. Acoustic field of a single vehicle on the road

The basic hypothesis in the current formulation is that the vehicle could be regarded as a point sound

source or acoustic monopole. This means that the directivity of the vehicle noise is dropped in the first place. However, unlike aircraft, the vehicle does not operate in free space but on the road and moves along a certain direction with variable speed. Therefore, the reflection effect of the ground and the moving effect of the vehicle on sound propagation should not be neglected.

With the above considerations, the vehicle on the road is modeled as a moving point sound source in half-space. Figure 1a sketches the geometric configuration of the observation point (X_o, Y_o, Z_o, t) and the i-th vehicle (in red) on the road (X_i, Y_i, Z_i, t) at time t. The formulation starts from the three-dimensional sound pressure field expression of a static point source at frequency f. At time t the acoustic pressure at the observation point is (Smith III, 2010)

$$p_s(X_o, Y_o, Z_o, t) = \frac{p_a}{r_{io}} e^{i(2\pi f t - k r_{io})}, \tag{1}$$

where p_a represents the acoustic pressure amplitude of the point sound source, f and k are the frequency and the wavenumber of the sound wave, and r_{io} is the distance between the sound source and the observation point. In Eq. (1), the pressure variable whose amplitude is proportional to $1/r$ with propagation distance (Smith III, 2010) is used instead of the acoustic intensity, which follows the inverse square law in order to consider the phase difference when superimposing the contribution of all the vehicles on the road in Eq. (3).

The moving effect means that the measurement of acoustic pressure at the observation point at the moment t does not come directly from the vehicle's current position at t (red vehicle in Fig. 1a) but from a certain moment prior to t at the position of $(X_i - V_i\tau, Y_i, Z_i, t-\tau)$ (upward pink vehicle in Fig. 1a). This difference in time is called the retarded time τ or delay. To estimate it, the simplified sketch in Fig. 1b should be referred to. The first step is to calculate the orientation angle θ. According to the dot product of vector $\overrightarrow{A'A}$ and $\overrightarrow{AO}$, the orientation angle is

$$\theta = \arccos\left(\frac{\overrightarrow{A'A}\, g\, \overrightarrow{AO}}{\left|\overrightarrow{A'A}\right|\left|\overrightarrow{AO}\right|}\right), \tag{2}$$

where $\overrightarrow{AO}$ is the vector from the vehicle's current position to the observation point at time t. $\overrightarrow{A'A}$ is the distance traveled by the i-th vehicle during the retarded time. In Eq. (2), since the retarded time τ is unknown, the direction of the vector $A'A$ is sufficient for the calculation.

After obtaining the orientation angle θ, it is possible to derive the retarded time τ. During the retarded time, the vehicle has traveled a distance of $\left|\overrightarrow{A'A}\right| = V_i\tau$ if its speed was assumed constant during that period. Let us take the triangle $\Delta OAA'$, the cosine theorem says:

$$(c_0\tau)^2 = (V_i\tau)^2 + \left|\overrightarrow{OA}\right|^2 - 2\,(V_i\tau)\left|\overrightarrow{OA}\right|\cos(\theta), \tag{3}$$

where c_0 is the speed of sound and V_i is the speed of the i-th vehicle. By solving this second degree equation, the retarded time τ is obtained so that the exact position of the i-th vehicle at time $t-\tau$ is derived as $A' = (X_i - V_i\tau, Y_i, Z_i, t-\tau)$.

The ground effect means that the sound traveling downwards z-direction is reflected by the road surface. This effect is treated by adding an image point source beneath the road (Hudson, 2008; McLaughlin *et al.*, 2008), as shown in Fig. 1b by an upside-down pink vehicle. Mathematically, the position of the image point source is $A'' = (X_i - V_i\tau, Y_i, -Z_i, t-\tau)$. The strength of the image source varies with different types of road surface due to different sound reflection and absorption coefficients.

With the moving point sound source and the ground effect, the acoustic pressure of frequency f at

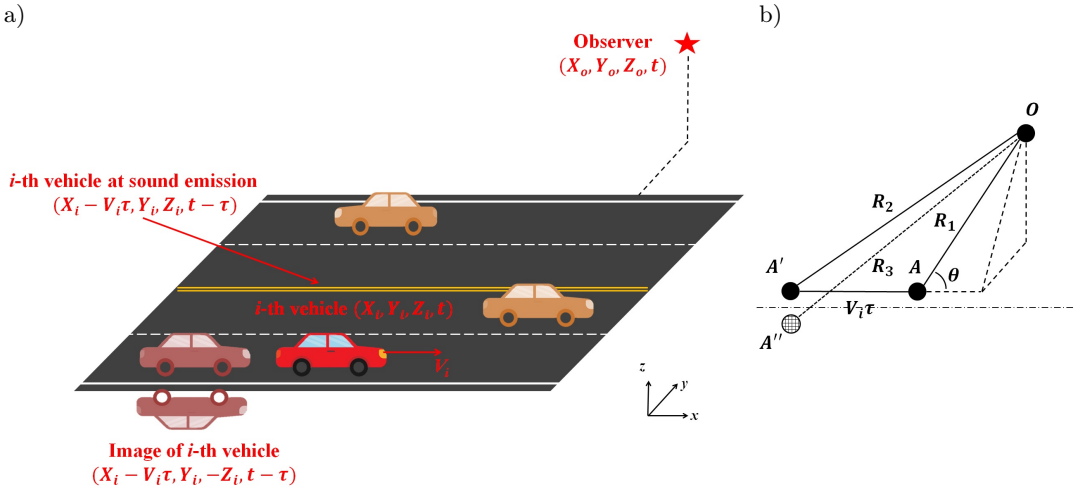

Fig. 1. Schematic representation of the formulation: a) geometry configuration; b) simplified sketch.

the observation point at time t caused by the i-th vehicle is the sum of the two point sources located at $A' = (X_i - V_i\tau, Y_i, Z_i, t-\tau)$ and $A'' = (X_i - V_i\tau, Y_i, -Z_i, t-\tau)$.

$$p_o^i(X_oY_oZ_ot) = \frac{p_a^i}{R_2}e^{i(2\pi f(t-\tau)-kR_2)} + \frac{C_g(f)p_a^i}{R_3}e^{i(2\pi f(t-\tau)-kR_3)}, \quad (4)$$

where $R_2 = |OA'|$ is the distance between the i-th vehicle at the moment of sound emission $t-\tau$ and the observer point, and $R_3 = |OA''|$ is the distance between the image of the i-th vehicle and the observer point. The coefficient $C_g(f)$ stands for the frequency-dependent reflection coefficient of the ground surface. In the current paper, it is set according to the measured absorption coefficients of asphalt pavements in the work of Knabben *et al.* (2016) and Li *et al.* (2014). Detailed values of the reflection coefficient are listed in Appendix A.

2.2. Vehicle noise source characteristics

Subsection 2.1 derived a formulation that could calculate the acoustic pressure field of a single moving vehicle on the road. However, in Eq. (4), the acoustic pressure amplitude p_a is dependent on the strength of the sound source. The dependence of this variable on vehicle type, speed and frequency requires the support of field data. In this paper, we are not engaged in collecting vehicle noise source characteristics but in using the source model of Lin *et al.* (2012) and the single vehicle noise spectral characteristics in the work of Yang *et al.* (2020). A brief introduction and the use of the employed models are presented herein for completeness.

According to Lin *et al.* (2012), the sound pressure level of a vehicle at the reference location 7.5 m away from the first lane and 1.2 m in height is dependent on its speed and vehicle type by:

$$\begin{aligned} \text{light vehicle:} \quad & L = 27.96 + 24.91\log 10(V), \\ \text{medium vehicle:} \quad & L = 28.36 + 29.73\log 10(V), \\ \text{heavy vehicle:} \quad & L = 31.77 + 29.70\log 10(V), \end{aligned} \quad (5)$$

where V is the speed of the vehicle in km/h. Lin *et al.* (2012) expression establishes the relationship between vehicle noise pressure level and vehicle speed based on vehicle type. It means that the acoustic pressure amplitude could be written as $p_a^i(\text{Type}_i, V_i)$. However, Lin's expression (Lin *et al.*, 2012) is only valid for the overall sound pressure level that does not contain spectral energy distribution.

In (Yang *et al.*, 2020) detailed noise spectral energy distribution at 1/3 octave frequencies from 12.5 Hz to 20 kHz is provided for four types of vehicles: light vehicle, medium vehicle, heavy vehicle, and bus. Since the vehicle speed also influences the spectral energy distribution, Yang *et al.* (2020) have also provided the noise spectral energy distribution at different velocity intervals. By collecting the spectral information the authors of this paper have established a database for four vehicle types and five vehicle speed intervals at 28 1/3 octave frequency bands. Detailed spectral distributions can be found in Appendix B.

To combine the model of Lin *et al.* (2012) and the data of Yang *et al.* (2020), the acoustic pressure amplitude p_a at frequency f_k for a certain type of vehicle at velocity V_i is the multiplication of the sound pressure (converted from sound pressure level) from Eq. (5) and the spectral energy distribution at frequency f_k. Finally, the acoustic pressure amplitude in Eq. (4) is dependent on vehicle type, speed and frequency $p_a^i(\text{Type}_i, V_i, f_k)$. It should be pointed out that although the field data in the literature was acquired by experimental measurements, the absolute amplitude of $p_a^i(\text{Type}_i, V_i, f_k)$ still needs to be calibrated for realistic application. This is because the exact values of the first terms in Eq. (5) (Lin's expression (Lin *et al.*, 2012)) depend on the reference location of the measurement.

2.3. Prediction of traffic flow noise on the road

With the formulation of the acoustic field of a single vehicle and the vehicle noise feature database, it is possible to evaluate the total noise spectrum of the whole traffic flow on the road. At a given observation point position and time (X_o, Y_o, Z_o, t), the total acoustic pressure p_{total} at one of the 1/3 octave frequency bands f_k is the sum of the contribution of each vehicle on the road:

$$p_{\text{total}}(X_o, Y_o, Z_o, t, f_k) = \sum_i \left(\frac{p_a^i(\text{Type}_i, V_i, f_k)}{R_2} e^{i(2\pi f_k(t-\tau)-kR_2)} + \frac{C_g p_a^i(\text{Type}_i, V_i, f_k)}{R_3} e^{i(2\pi f_k(t-\tau)-kR_3)} \right), \quad (6)$$

where i represents the i-th vehicle on the road, and k is the k-th 1/3 octave frequency band. To obtain the noise spectrum at the observation point, the total acoustic pressure p_{total} at every 1/3 octave frequency band should be calculated following Eq. (6).

To derive the sound pressure level spectra, the sound pressure level at each frequency band SPL(f_k) is calculated first with the A-weighting factor. Then, considering that vegetation by the side of the arterial roads could attenuate sound that passes, sound attenuation through trees should be accounted for when calculating the sound pressure level spectra in the far field (Van Renterghem *et al.*, 2012). Figure 2 shows a schematic configuration when calculating the sound

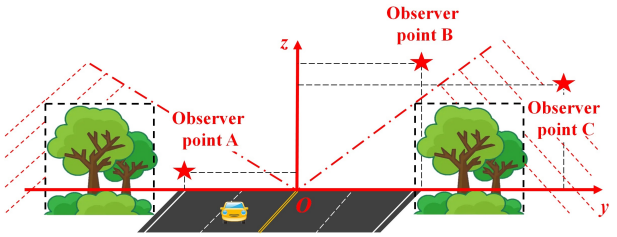

Fig. 2. Schematic configuration for sound attenuation calculation by vegetation.

attenuation by vegetation on a certain cross-section plane of the road. The origin of the cross-section plane is placed on the road's centerline, where the noise source location is assumed. For the observer points in the dashed line region, the attenuation of the trees is accounted for because the trees would block the sound propagating directly from the source to the observers, such as the far-field observer point C in the figure. However, for far-field observer point B and near-field observer point A, the sound attenuation by the vegetation needs not to be counted. Detailed sound attenuation values employ those in (PRICE *et al.*, 1988), as listed in Appendix C.

2.4. Comments on the proposed traffic noise prediction method

The proposed traffic noise prediction method is based on the acoustic pressure field of moving point sources in half-space and the field data of vehicle noise from the literature, as explained in Subsecs. 2.1 and 2.2. These two elements are independent of the traffic flow status because they deal only with one vehicle. However, the traffic flow on arterial roads contains hundreds to thousands of vehicles. The summation in Eq. (6) is mathematically rigid but not easy to be applied in real circumstances since it demands the time-dependent position and velocity of every vehicle on the road.

In real circumstances, traffic noise from arterial roads is more important at rush hours during the day because of the very high traffic volume. During rush hours, the traffic volume is not only high, but also steady and uniform. This means that all the vehicles on the road are driven at a relatively high and steady speed, and the gaps between vehicles are nearly uniform. Under this condition, the lane-wise time-averaged vehicle speed and volume could be a good approximation of the realistic traffic scenarios. As it could represent the main feature of the traffic flow on the road and it does not demand every detail of the traffic flow. Therefore, to apply the proposed method to realistic traffic noise prediction problems, we could first obtain lane-wise traffic data by field measurements during rush hours. Then establish numerically an equivalent traffic flow calculated from the lane-wise measurement data. With the equivalent traffic flow established, the position and the velocity of each vehicle in the traffic flow could be derived so that the formulation in Subsecs. 2.1, 2.2, and 2.3 could be applied to calculate the noise spectra from the whole segment of the road at a certain observation point.

3. Calibration and validation

In order to validate the proposed method, a field measurement is conducted, obtaining four groups of traffic flow and roadside noise data. The logic behind is to use one group of the data to calibrate the absolute value of the acoustic pressure amplitude $p_a^i(\mathrm{Type}_i, V_i, f_k)$ in Eq. (6) and use the other three groups for validation.

3.1. Test site

The test site is chosen to be a segment of Jingshi Road, Jinan, China. It is a two-way 14-lane arterial road that is the most important road in Jinan city. Near Jingshi Road, three residential districts, business buildings, hotels, and hospitals are located. During rush hours, due to the very high traffic flow volume, the traffic noise is very explicit and impacts the people who live and work in the buildings by the road.

As shown in Fig. 3a, the length of the tested road segment is about 1.2 km. The observation points are

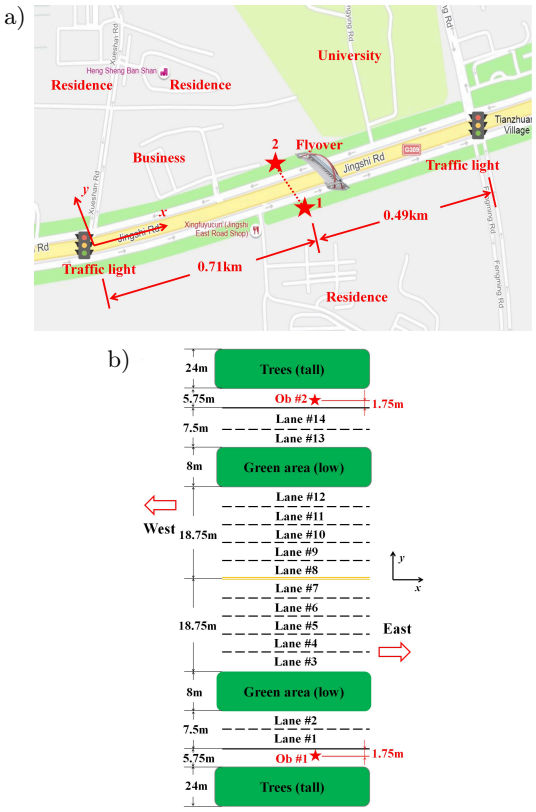

Fig. 3. Spatial configuration of the test site: a) overall geometry of the tested road segment; b) lane definition of the tested road segment.

chosen to be near the middle of the tested segment to make sure that the vehicles' speeds passing the observation points reached a quasi-steady state. A flyover bridge is located near the observation points where the video of the traffic flow is taken. The road has 14 lanes and 2 green areas. The width of each lane is 3.75 m and that of the green area is approximately 8 m. On both sides of the road, there are two belts of barrier trees. These barrier trees, consisting of a mixture of poplar (Populus simonii), cypress, and Chinese holly (Ilex cornuta), are 40 m away from the road's centerline and have a width of 24 m and a height of about 20 m. The total road width is 68.5 m including the automotive lanes only, and 128 m including the pedestrian lanes and barrier trees. The road direction is chosen to be along the x-direction in the formulation. The origin is at the west end of the road segment. The road width direction is the y-direction, originating at the road's centerline. The lane is numbered from south to north, as shown in Fig. 3b.

The test was conducted on May 30th, 2021, during rush hour from 5:30 pm to 6 pm (sunny, local temperature 25° (Hourly Historical Weather Data [OL])). Four groups of traffic flow and roadside noise data were collected. For group #1 and group #2, the noise measurement was conducted at point 1 (710 m, −36 m, 1.6 m), which is 1.75 m to the southern edge of lane #1 and at the height of 1.6 m, as shown in Fig. 3a. For group #3 and group #4, the observation location was on the other side of the road at point 2 (710 m, 36 m, 1.6 m), as shown in Fig. 3a. The sound pressure levels at 1/3 octave frequencies were recorded at the observation points.

3.2. Lane-wise average traffic flow volume and speed

The traffic volume on the tested road segment is wavy in time due to the traffic lights being located at the two ends (Fig. 3a). In reality, the traffic noise is crucial only when the traffic volume is high. Therefore, we choose to record the noise and flow data only when the traffic flow volume is high and steady. This corresponds to a duration of about 40 s for each group of measurement where the green lights are on (the green cycle is 120 s) and the vehicles passing the observation points reach relatively high and steady speeds. By analyzing the videos of the traffic flow, the traffic volume and average speed on each of the 14 lanes could be derived. Detailed traffic flow data are listed in Table 1.

In the measured traffic flow data, group #1 and group #2, focusing on the traffic from west to east, have comparable traffic volumes of 12690 veh/h and 13050 veh/h. Group #3 and group #4, focusing on the other direction, have comparable traffic volumes of 14130 veh/h and 14490 veh/h. The aforementioned traffic volumes are the total volume of both directions, and the difference is due to the measurement time, where the first two groups were measured between 5:30 pm to 5:45 pm and the last two groups were measured between 5:45 pm to 6 pm. As for vehicle type, most vehicles moving on the road during this period of time are light vehicles and buses. No heavy trucks were found. In terms of the lane-wise data, traffic volume is high in middle lanes (#4, #5, #6 and #9, #10, #11) for both directions and the speed is high in the fast lanes (#7 and #8). For the lanes near the roadside (#1 and #14), the traffic volumes and speeds are

Table 1. Lane-wise traffic flow data of group #1, group #2, group #3, group #4 (separated by slash sign).

Group #1/Group#2/Group #3/Group #4					
Lane	Traffic volume [veh/h]			Lane speed [km/h]	Lane gap [m]
	Light vehicle	Medium vehicle	Bus		
#1	90/90/90/90	0/0/0/0	0/0/0/0	27/20/20/20	300/222.2/222.2/222.2
#2	720/810/810/810	0/0/90/0	90/0/270/90	36/36/36/32	44.44/44.44/30.77/35.56
#3	900/810/540/1260	0/0/0/0	90/0/90/0	48/52/52/52	48.48/64.20/82.54/41.27
#4	1350/990/1350/1170	0/90/0/0	0/90/0/0	54/56/56/52	40.00/47.86/41.48/44.44
#5	1350/1530/1710/1440	0/0/0/0	0/0/0/0	54/56/56/56	40.00/36.60/32.75/38.89
#6	990/1170/1350/1530	90/0/0/0	0/0/0/0	54/56/56/56	50.00/47.86/41.48/36.60
#7	990/720/720/1080	0/0/0/0	0/0/0/0	60/54/54/60	60.61/75.00/75.00/55.56
#8	990/1260/900/1350	0/0/0/0	0/0/0/0	58/58/60/62	58.59/46.03/66.67/45.93
#9	1260/1170/1530/1080	0/0/0/0	0/0/0/0	52/54/56/54	41.27/46.15/36.60/50.00
#10	900/1080/1530/1350	90/0/0/0	0/90/0/0	52/58/54/54	52.53/49.57/35.29/40.00
#11	1530/1080/990/1350	0/90/0/0	0/0/90/180	58/54/54/51	37.91/46.15/50.00/33.33
#12	360/360/1080/720	0/0/0/0	0/450/90/90	50/48/52/50	138.9/59.26/44.44/61.73
#13	720/1080/720/810	0/0/0/0	180/90/90/90	40/42/48/48	44.44/35.90/59.26/53.33
#14	0/0/0/0	0/0/0/0	0/0/90/0	0/0/45/0	–/–/500/–
Total	12690/13050/14130/14490				

very low. This phenomenon has two reasons. The first reason is that during rush hours, these two lanes are reserved only for buses and other vehicles are allowed to use them only for taking turns. The other reason is that electric and traditional motorcycles on the road nearly block the side lanes at rush hour, so buses can only take the lanes next to the side lanes.

3.3. Equivalent traffic flow

Based on the time-averaged lane-wise traffic flow data in Table 1, the equivalent steady traffic flow could be established numerically. In this equivalent traffic flow, vehicles on the same lane have identical speed and vehicle gap. The total number of vehicles depends on the traffic volume values. The type of vehicle also depends on the lane-wise percentage.

As mentioned above, each vehicle is regarded as a moving point sound source in half space. The vehicles are set to be moving at constant speed along the centerline of each lane. The z-coordinates of the sound source of vehicles depend on its type. For light, medium, and heavy vehicles and buses, the heights of the point sound sources are set to $z = 0.5$ m, 0.7 m, 1.0 m, and 1.0 m, respectively. A simple geometric configuration of vehicles on the road and the observer in the far field is shown in Fig. 4. In accordance with the field measurements, the duration of the equivalent traffic flow in the predictions is also set to 40 s.

3.4. Roadside traffic noise

The roadside traffic noise was measured simultaneously with the traffic flow. By averaging the measured noise data, the time-averaged noise spectra and the overall sound pressure levels could be derived for each group of measurement. As previously pointed out, the data of group #1 is used to calibrate the method and the other three groups' data are used for validation.

3.4.1. Calibration of the formulation

Since the observer-to-road distances are different in Lin's equations (Lin *et al.*, 2012) and in the current measurement, the constant values need to be calibrated. By shifting the constant values in Eq. (5) by −1.94 dB, the measured and predicted traffic noise spectra are shown in Fig. 5. It can be seen in the figure that the predicted spectrum approximates the measured one within an error band of 3 dB between 400–6000 Hz where the sound pressure level is high. The error band in the measurements is 3 dB, because during the field measurement, randomly-occurred noise sources such as motorcycles, walking-by pedestrians and wind would alter the sound levels at the observation points and thus influencing the consistency of the measurement results. The A-weighted overall sound pressure level calculated from the prediction is 67.3 dBA, while the measured value is 67.7 dBA. Therefore, it is believed that under this parameter setting, the prediction is close enough to the measurement where the shifting value in Eq. (5) is −1.94 dB. These parameters are fixed and are employed to check whether the predictions by the proposed method could well approximate the other field measurements.

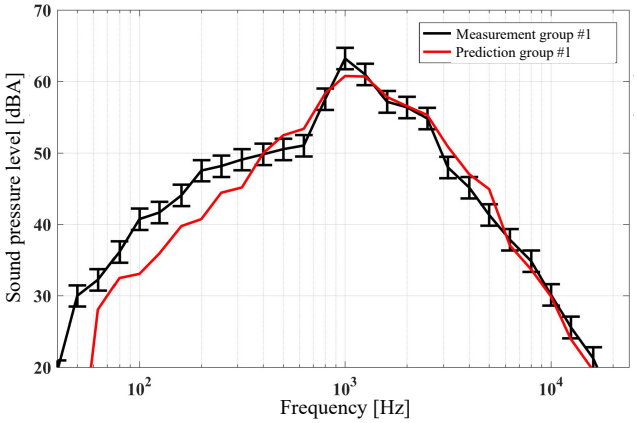

Fig. 5. Comparison of measured and predicted traffic noise spectrum for group #1 (error band for the measurement is 3 dB).

3.4.2. Validation of the method

With the calibrated formulation and the measured traffic flow data of group #2, group #3, and group #4, the noise generated by the traffic flow could be estimated and compared with the measured noise. Figure 6 compares the measured and predicted noise spectra.

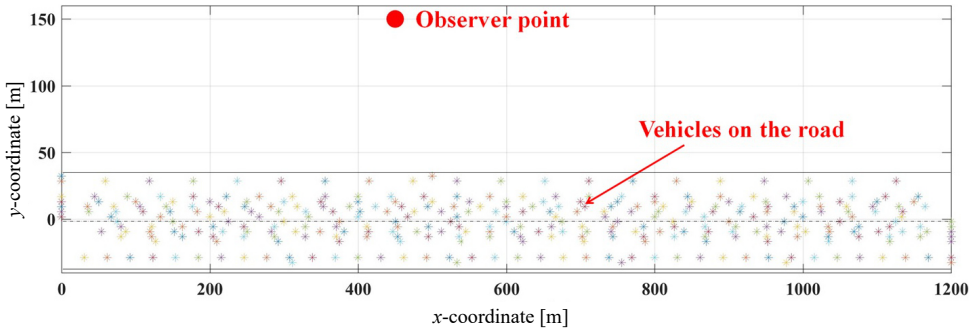

Fig. 4. Geometric configuration of the vehicles on the road and the observer point (each * represents one vehicle).

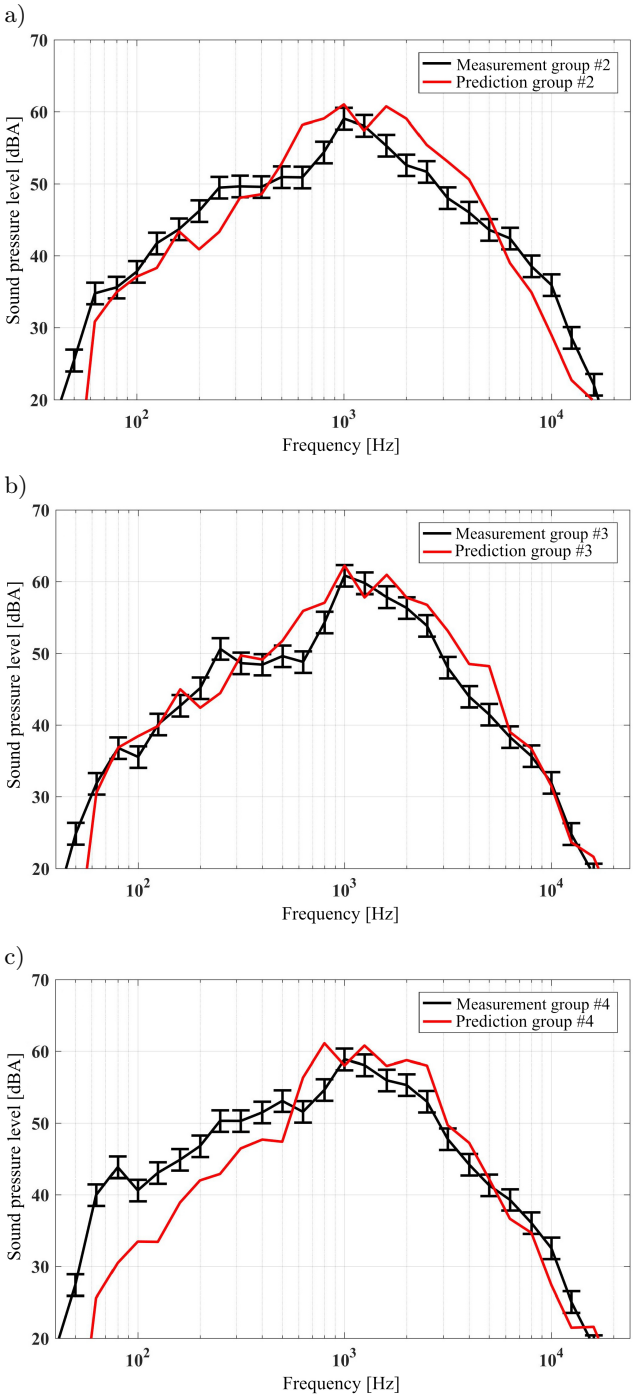

Fig. 6. Comparison of measured and predicted traffic noise spectrum for: a) group #2; b) group #3; c) group #4 (error band for the measurement is 3 dB).

For group #2 in Fig. 6a, the predicted spectrum approximates the measurement quite well. At some 1/3 frequency bands from 100 Hz to 6000 Hz, the differences in sound pressure level exceed the error band of 3 dB but are mostly less than 5 dB. For group #3 and group #4, where the noise measurement point is on the other side of the road, the predicted spectra seem to be even closer to the measurements than the calibration group. Especially for group #3, the differences in sound pressure level from 50 Hz to 6000 Hz are mostly within the error band of 3 dB.

In terms of the overall sound pressure level, the predicted values are 67.3 dBA, 68.0 dBA, 68.0 dBA, and 67.7 dBA for group #1, group #2, group #3, and group #4, while the measured values are 67.7 dBA, 65.0 dBA, 66.5 dBA, and 65.3 dBA. The differences in the overall sound pressure level are −0. dB, 3.0 dB, 1.5 dB, and 2.4 dB, respectively. The four groups' overall sound pressure level differences are less than 3 dB.

Table 2. Comparison of the overall sound pressure level.

Purpose	Calibration	Validation		
Group number	#1	#2	#3	#4
Measurement	67.7 dBA	65.0 dBA	66.5 dBA	65.3 dBA
Prediction	67.3 dBA	68.0 dBA	68.0 dBA	67.7 dBA
SPL difference	−0.4 dB	3.0 dB	1.5 dB	2.4 dB

4. Prediction of roadside noise in different scenarios

In Sec. 3, the proposed traffic noise prediction method was calibrated and validated by field measurements. The predicted and the measured overall sound pressure levels and spectra show good coherence. On this basis, we intend to investigate the influence of traffic noise on people who live and work alongside arterial roads. This means more attention will be paid to the sound field distribution in the far field.

Of all the traffic scenarios, two are considered an obvious annoyance. The first one is during rush hours, when the impact of traffic noise is quite severe due to the high traffic volume on the road. Then it is interesting to know how the traffic noise evolves with traffic volume and vehicle average speed. The second scenario is near midnight when people are about to fall asleep. During this period of time, there are frequently fully-loaded heavy-duty trucks running on the road because trucks are not allowed to enter the urban area during daytime due to local traffic regulations. Since the traffic volume is low during that period, these heavy trucks tend to be driven at very elevated speeds generating high-level noise.

Therefore, this section intends to employ the previously established method to study the far-field traffic noise of the above two scenarios.

4.1. Roadside noise distribution during rush hours

In Subsec. 3.4.2, since the predicted and the measured spectra are the closest for group #3 (Fig. 6b) among group #2, group #3, and group #4, we employ the equivalent traffic flow established from the data of this group to represent the traffic flow during rush hours. Near the middle of the road segment (x = 710 m), a cross-section observation plane is set up,

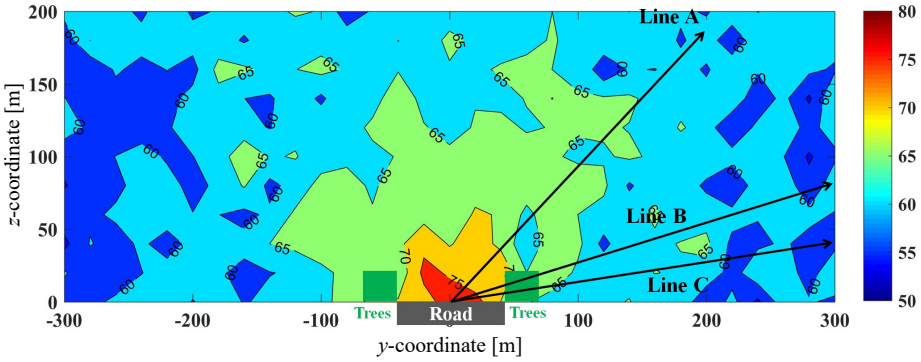

Fig. 7. Overall time-averaged A-weighted sound pressure level on cross-section observation plane (grid size 20 × 20 m).

which is 600 m in width (y-direction) and 200 m in height (z-direction).

With the equivalent traffic flow and the proposed traffic noise prediction method, the overall time-averaged A-weighted sound pressure level on the observation plane is calculated (Fig. 7). From the predicted results, it can be seen that traffic noise at rush hours on the tested road is quite strong. In the region between the two tree belts and within 100 m from the road centerline, the maximum overall sound pressure level could reach as high as 74.3 dBA, and the minimum value is no less than 65 dBA. The far-field noise level distribution has a sort of directivity due to the attenuation of the trees on both sides of the road. In the region "behind" the trees, the noise pressure level is reduced significantly.

To provide a detailed evolution of noise level with distance, the overall time-averaged A-weighted sound pressure level as a function of distance away from the road centerline is drawn in Fig. 8 along the directions of the arrows in Fig. 7. The angles between the arrow and positive y-axis for line A, line B, and line C are 45°, 18.43°, and 9.46°, respectively. It can be noted that the traffic noise level decreases with distance. Starting from 50 m, for the direction of line B and line C, due to the attenuation of the trees, the overall sound pressure levels are 2–3 dB lower than that along line A.

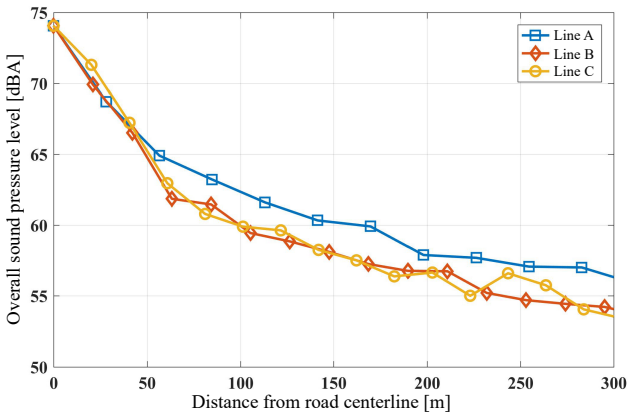

Fig. 8. Overall time-averaged A-weighted sound pressure level as a function of distance from the road centerline.

Figure 9 plots the predicted noise spectrum at a far-field observation point of (450, 350, and 100 m). This far-field point represent the location of the windows of the nearest high-rise residential buildings by the road. It can be seen that the sound pressure level exceeds 40.0 dBA during rush hours for a frequency range between 630 Hz to 2500 Hz. The overall predicted sound pressure level at this point is 53.2 dBA.

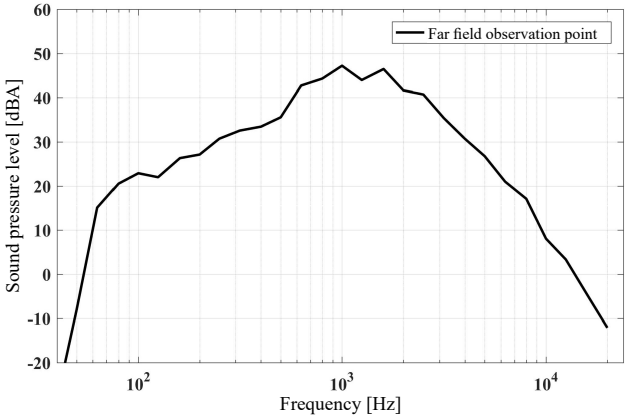

Fig. 9. Noise spectrum at far-field observation point (450, 350, and 100 m).

4.2. Traffic noise evolution with traffic volume

Besides rush hours, it is also interesting to know the traffic noise evolution when the traffic volume varies. In this section, we are going to test different traffic volumes. The equivalent traffic flow is also based on the data of group #3. The total traffic volume on the road is set to be 7065 veh/h, 10598 veh/h, 14130 veh/h, and 17663 veh/h, corresponding to 50%, 75%, 100%, 125% of that in group #3.

Figure 10 shows the predicted overall time-averaged A-weighted sound pressure level on the cross-section observation plane at x = 710 m for the traffic volume of 7065 veh/h, 10598 veh/h, and 17663 veh/h (the 14130 veh/h case is shown in Fig. 7). As the traffic volume increases, the maximum A-weighted overall sound pressure level near the road increases from 70.1 dBA to 73.5 dBA to 74.3 dBA and to 75.0 dBA.

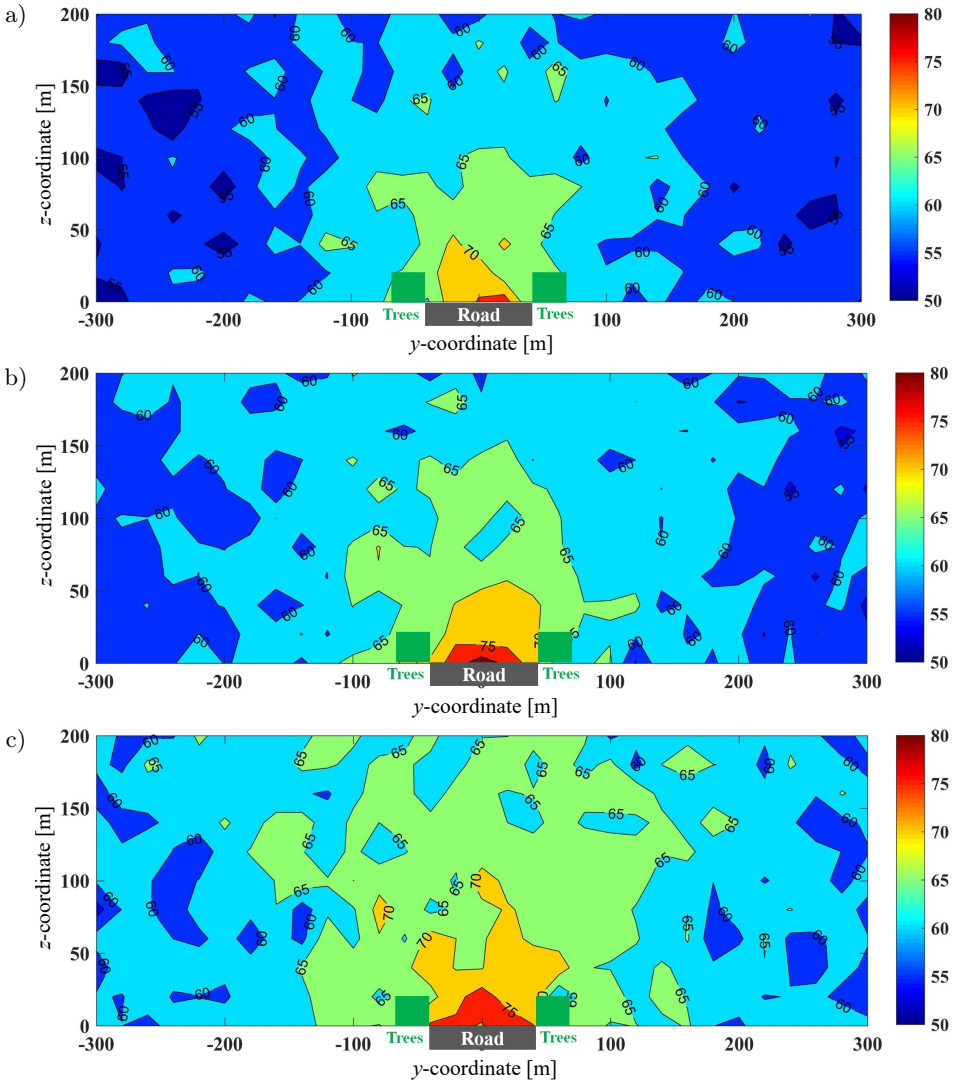

Fig. 10. Overall time-averaged A-weighted sound pressure level on cross-section observation plane at $x = 710$ m: a) 7065 veh/h; b) 10598 veh/h; c) 17663 veh/h (grid size 20×20 m).

Figure 11 compares the spatial evolution of the overall A-weighted sound pressure level at different traffic volumes along line B in Fig. 7. From a traffic volume of 7065 veh/h, each increase of 3533 veh/h would bring an increase in the overall sound pressure level of about 1.8 dB, 1.3 dB, and 1.0 dB, respectively.

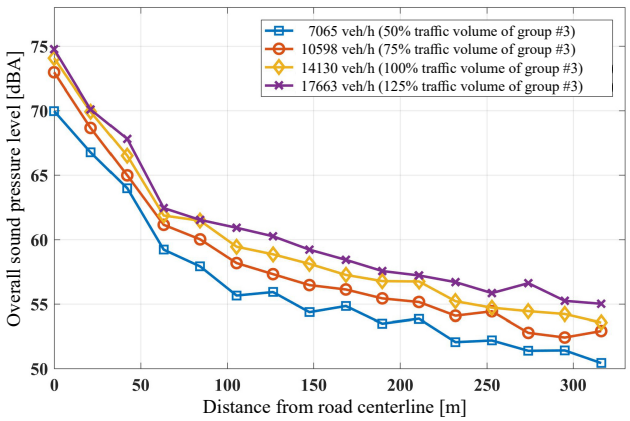

Fig. 11. Overall time-averaged A-weighted sound pressure level as a function of distance from the road centerline (along line B in Fig. 7) at different traffic volumes.

4.3. Traffic noise evolution with vehicle speed

In this section, the influence of the average vehicle speed on traffic noise is tested. To make a comparison, the lane-wise average vehicle speeds in group #3 are multiplied by a ratio of 0.75, 1, and 1.25, making an average speed of 37.45, 49.93, and 62.41 km/h.

Figure 12 shows the predicted overall time-averaged A-weighted sound pressure level on the cross-section observation plane at $x = 710$ m for the average speed of 37.45 km/h and 62.41 km/h (the 49.93 km/h case is shown in Fig. 7). It can be seen that with higher average vehicle speed, the traffic noise level becomes higher. The maximum A-weighted overall sound pres-

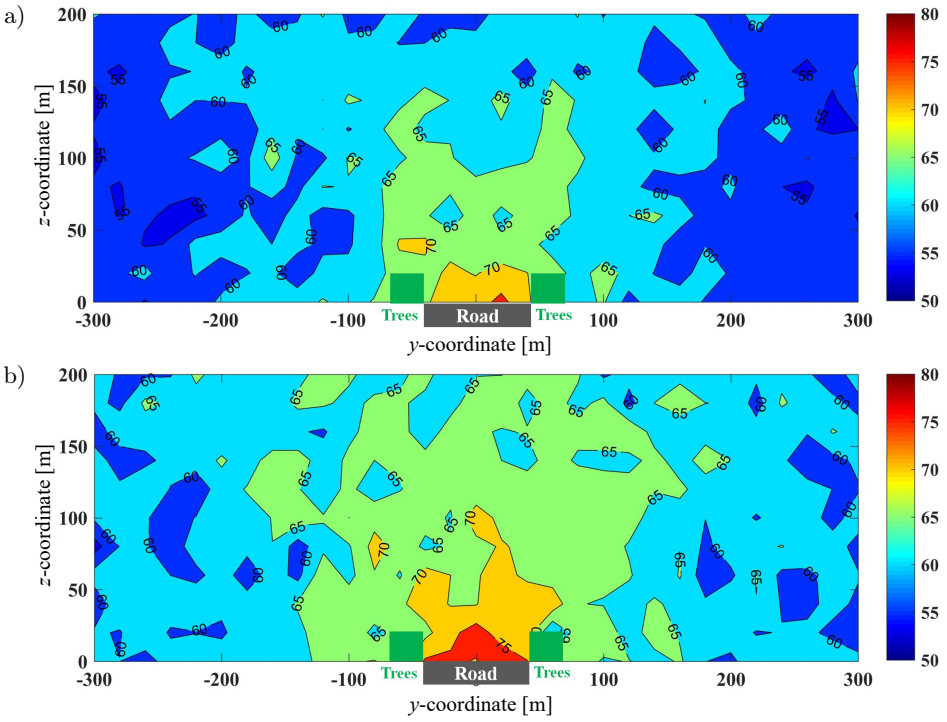

Fig. 12. Overall time-averaged A-weighted sound pressure level on cross-section observation plane at x = 710 m: a) 37.45 km/h; b) 62.41 km/h (grid size 20 × 20 m).

sure level near the road increases from 72.0 dBA to 74.3 dBA and to 77.5 dBA with increasing speed.

To quantify the influence of traffic flow speed, the spatial evolution of the overall A-weighted sound pressure level at different average vehicle speeds are compared in Fig. 13. The mean difference in decibel between the 37.45 km/h case and the 49.93 km/h case is 1.7 dB and that between the 50.31 km/h case and the 62.41 km/h case is 2.2 dB.

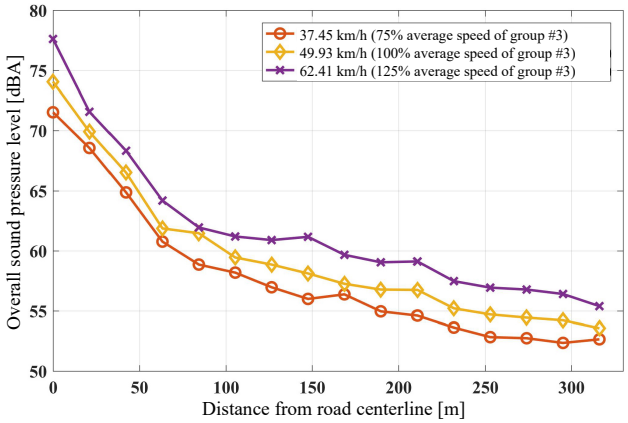

Fig. 13. Overall time-averaged A-weighted sound pressure level as a function of distance from the road centerline at different vehicle speeds.

4.4. Traffic noise from heavy trucks

Finally, the midnight scenario dominated by heavy-duty trucks' noise is studied. We name this case group #5. During mid-night on Jingshi Road, except for heavy trucks, there are still occasionally light vehicles, but medium vehicles and buses are rare. Since the traffic volume is low, the vehicles on the road tend to be driven at full speeds. The speed limit on Jingshi Road is 80 km/h and the speed limit for trucks is 50 km/h within urban areas. Based on these considerations, the traffic flow for group #5 is presented in Table 3. In this case, heavy trucks having a lane-wise volume of 360 veh/h exist on lane #2, #3, #4, #11, #12, and #13 at the limit speed of 50 km/h. On the other lanes of the road exists a certain number of light vehicles at 80 km/h. The total traffic volume is 3420 veh/h for both directions.

Figure 14 plots the predicted overall time-averaged A-weighted sound pressure level distribution on the cross-section observation plane at x = 710 m. Compared with previously tested cases, the truck-dominated case is as 'noisy' as the group #3 case in Fig. 7. In the region near the road, the maximum A-weighted overall sound pressure level for group #5 is 73.5 dBA and that of group #3 is 74.3 dBA.

Since the noise characteristics depend on vehicle type, the noise spectral feature could be different even with the same value of sound pressure level. Figure 15 compares the spectra of the two cases. It is observed that for the truck-dominated case, the contribution at low frequencies is more important. Between 100 Hz and 200 Hz, the noise level emitted by trucks is 5 dB higher than for a mixed type of vehicles. The overall A-weighted sound pressure level for group #5 is

Table 3. Lane-wise traffic flow data of group #5.

Group #5						
Lane number	Traffic volume [veh/h]				Lane speed [km/h]	Lane gap [m]
	Light vehicle	Medium vehicle	Heavy vehicle	Bus		
#1	90	0	0	0	30	333.33
#2	0	0	360	0	50	138.89
#3	0	0	360	0	50	138.89
#4	0	0	360	0	50	138.89
#5	180	0	0	0	80	444.44
#6	180	0	0	0	80	444.44
#7	180	0	0	0	80	444.44
#8	180	0	0	0	80	444.44
#9	180	0	0	0	80	444.44
#10	180	0	0	0	80	444.44
#11	0	0	360	0	50	138.89
#12	0	0	360	0	50	138.89
#13	0	0	360	0	50	138.89
#14	90	0	0	0	30	333.33
	3420 (total)					

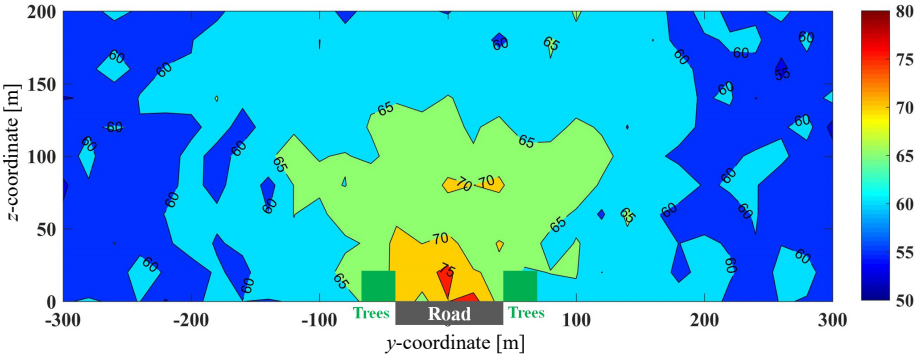

Fig. 14. Overall time-averaged A-weighted sound pressure level on cross-section observation plane at $x = 710$ m for the heavy truck-dominated case (grid size 20×20 m).

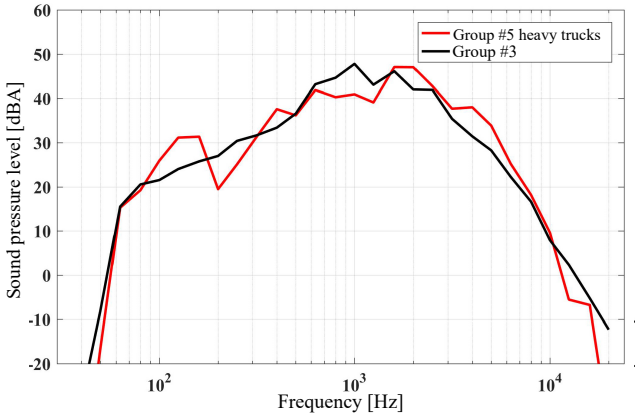

Fig. 15. Noise spectra at far-field observation point (450 m, 350 m, 100 m) for the truck-dominated case and that of group #3 case.

52.9 dBA, while that of group #3 at the same observation point is 53.2 dBA.

5. Conclusions

Focusing on the influence of traffic noise from arterial roads on people in nearby high-rise buildings, this paper proposes and validates a microscopic-level noise prediction method that could estimate the spatial distribution and spectral characteristics of traffic noise in the vicinity of multi-lane arterial roads.

In the prediction method, the sound pressure field for each vehicle could account for the motion of the vehicle and the reflection effect of the ground. With lane-wise field data as input, an equivalent traffic flow could be established to model the road as a multiple-lane noise source. Accompanied by the noise source model and spectral characteristics in the literature, the method is able to evaluate the spectral and total sound pressure level at a certain observer point by superimposing the individual contribution of all the vehicles on the road. The proposed method is only applicable

to noise issues near city arterial roads where the linear source assumption of the traffic flow does not hold.

To validate the proposed method, a field measurement on a segment of Jingshi Road, Jinan, China, was conducted, obtaining four groups of traffic flow and noise data. The data of group #1 was employed to calibrate the formulation, whereas the other three groups were used for validation. The validation shows that, after calibration, the predicted overall sound pressure level could approximate the measured values by no more than 3 dB and the predicted noise spectra are within an error band of less than 5 dB for the frequency range between 500 Hz to 6000 Hz.

Based on the validated method, the roadside noise of some scenarios was studied. First, the traffic noise during rush hours was investigated. Prediction results show that the overall sound pressure level of the traffic flow during rush hours is over 60.0 dBA within a distance of 100 m from the road centerline. At a distance of 300 m, the noise level could still be as high as over 55.0 dBA. Then the influence of traffic volume and speed is investigated. The investigation shows that from a total traffic volume of 7065 veh/h to 17663 veh/h, each increase of 3533 veh/h would cause the overall sound pressure level to increase by 1.8 dB, 1.3 dB, and 1.0 dB, respectively. From an average traffic speed of 37.45 km/h to 62.41 km/h, each increase of 12.48 km/h would cause the overall sound pressure level to increase by 1.7 dB and 2.2 dB.

At last, a heavy truck-dominated scenario was studied. Prediction results show that at a total traffic volume of 3420 veh/h, the heavy truck-dominated scenario during the night could be as noisy as a total traffic volume of 14130 veh/h for a mixture of vehicles in the daytime. It was also found that the spectral contribution in the low-frequency range of 100 Hz and 200 Hz is more important for the heavy truck-dominated case.

The current paper demonstrates that the proposed method predicts traffic noise distribution near a segment of arterial road with a short-term quasi-steady traffic flow with a reasonable accuracy. However, the applicability and feasibility of the proposed method for long-term dynamic scenarios with detailed traffic flow data have not been investigated. Besides, some of the details in the modeling could be further extended, including the effect of sound attenuation of the ground (compacted field, loose ground, soft forest floor, etc.) and the effect of noise shielding of the vegetation belts (Van Renterghem *et al.*, 2012).

Acknowledgments

This research was supported by the Shandong Provincial Natural Science Foundations, China (Grants no. ZR2021QG061 and ZR2021QG150), the Doctoral Research Foundations of Shandong Jianzhu University, China (Grants no. X21108Z and X21107Z).

References

1. Barrigón Morillas J.M., Rey Gozalo G., Montes González D., Sánchez-Fernández M., Bachiller León A. (2022), A comprehensive experimental study of the influence of temperature on urban road traffic noise under real-world conditions, *Environmental Pollution*, **309**: 119761, doi: 10.1016/j.envpol.2022.119761.

2. Barry T.M., Reagan J.A. (1978), *FHWA highway traffic noise prediction model*, Washington: Department of Transportation, Federal Highway Administration National Technical Information Service.

3. Bendtsen H. (1999), The Nordic prediction method for road traffic noise, *Science of the Total Environment*, **235**(1–3): 331–338, doi: 10.1016/S0048-9697(99)00216-8.

4. CoRTN (1975), *Calculation of road traffic noise*, United Kingdom Department of the Environment and Welsh Office Joint Publication.

5. Directive EN (2015), *Commission Directive (EU) 2015/996 of 19 May 2015 establishing common noise assessment methods according to Directive 2002/49/EC of the European Parliament and of the Council*, http://data.europa.eu/eli/dir/2015/996/oj.

6. Dutilleux G. *et al.* (2010), NMPB-Route-2008: The revision of the French method for road traffic noise prediction, *Acta Acustica United with Acustica*, **96**(3): 452–462, doi: 10.3813/AAA.918298.

7. Hinton J., Jellyman A., Howell L.K. (2005), BUMP – The Birmingham updated noise mapping, *Forum Acusticum*, pp. 1003–1006.

8. Hourly Historical Weather Data [OL] (n.d.), https://www.weatherbit.io/history/hourly (access: 1.06.2021).

9. Hudson S. (2008), Ground reflection, *Lecture reference of Engineering for Telecommunications of Washington State University.*

10. Kaddoura I., Kröger L., Nagel K. (2017), An activity-based and dynamic approach to calculate road traffic noise damages, *Transportation Research Part D: Transport and Environment*, **54**: 335–347, doi: 10.1016/j.trd.2017.06.005.

11. Kephalopoulos S., Paviotti M., Anfosso-Lédée F. (2012), *Common Noise Assessment Methods in Europe (CNOSSOS-EU)*, EUR 25379 EN, Publications Office of the European Union, Luxembourg.

12. Khan J., Ketzel M., Jensen S.S., Gulliver J., Thysell E., Hertel O. (2021), Comparison of road traffic noise prediction models: CNOSSOS-EU, Nord 2000 and TRANEX, *Environmental Pollution*, **270**: 116240, doi: 10.1016/j.envpol.2020.116240.

13. Knabben K.M., Trichês G., Gerges S.N.Y., Vergara E.F. (2016), Evaluation of sound absorption capacity of asphalt mixtures, *Applied Acoustics*, **114**: 266–274, doi: 10.1016/j.apacoust.2016.08.008.

14. Lan Z., He C., Cai M. (2020), Urban road traffic noise spatiotemporal distribution mapping using multisource data, *Transportation Research Part D: Transport and Environment*, **82**: 102323, doi: 10.1016/j.trd.2020.102323.

15. Lee S.-W., Chang S.I., Park Y.-M. (2008), Utilizing noise mapping for environmental impact assessment in a downtown redevelopment area of Seoul, Korea, *Applied Acoustics*, **69**(8): 704–714, doi: 10.1016/j.apacoust.2007.02.009.

16. Li M., van Keulen W., van de Ven M., Molenaar A., Tang G. (2014), Investigation on material properties and surface characteristics related to tyre-road noise for thin layer surfacings, *Construction and Building Materials*, **59**: 62–71, doi: 10.1016/j.conbuildmat.2014.02.050.

17. Lin Y., Cai M., Li F. (2012), Studies on traffic noise source intensity regard for the acceleration, *Applied Acoustics (Chinese version)*, **31**: 282–286.

18. Lokhande S.K., Dhawale S.A., Pathak S.S., Gautam R., Jain M.C., Bodhe G.L., (2017), Appraisal of noise level dissemination surrounding mining and industrial areas of Keonjhar, Odisha: A comprehensive approach using noise mapping, *Archives of Acoustics*, **42**(3): 423–432, doi: 10.1515/aoa-2017-0044.

19. Lokhande S.K., Pathak S.S., Kokate P.A., Dhawale S.A. Bodhe G.L. (2018), Assessment of heterogeneous road traffic noise in Nagpur, *Archives of Acoustics*, **43**(1): 113–121, doi: 10.24425/118086.

20. Luo P., Cai M., Wang H. (2013), The noise spectral characteristics of various types of vehicles, *Noise and Vibration Control (Chinese version)*, **33**(5): 86–89.

21. McLaughlin D.K., Kuo C.-W., Papamoschou D. (2008), Experiments on the effect of ground reflections on supersonic jet noise, [in:] *46th AIAA Aerospace Sciences Meeting and Exhibit*, doi: 10.2514/6.2008-22.

22. Nielsen H.L. *et al.* (1996), *Road Traffic Noise – Nordic Prediction Method*, TemaNord 1996:525, Nordic Council of Ministers, Copenhagen, Denmark.

23. Peng J., Liu D., Parnell J., Kessissoglou N. (2019), Influence of translational vehicle dynamics on heavy vehicle noise emission, *Science of the Total Environment*, **689**: 1358–1369, doi: 10.1016/j.scitotenv.2019.06.426.

24. Popp C. (2003), Noise abatement planning in German-experiences and consequence of the EU directive on the assessment of environmental noise, *Acta Acustica United with Acustica*, **Suppl. 1**: 65–67.

25. Price M.A., Attenborough K., Heap N.W. (1988), Sound attenuation through trees: Measurements and models, *The Journal of the Acoustical Society of America*, **84**(5): 1836–1844, doi: 10.1121/1.397150.

26. Quartieri J. *et al.* (2009), A review of traffic noise predictive models, [in:] *Recent Advances in Applied and Theoretical Mechani Conference: Recent Advances in Applied and Theoretical Mechanics*, pp. 72–80.

27. RLS-90 (1990), *Guidelines for noise protection on roads* [in German: *Richtlinien für den Lärmschutz an Strassen],* Der Bundesminister Für Verkehr.

28. Sanok S. *et al.* (2022), Road traffic noise impacts sleep continuity in suburban residents: Exposure-response quantification of noise-induced awakenings from vehicle pass-bys at night, *Science of The Total Environment*, **817**: 152594, doi: 10.1016/j.scitotenv.2021.152594.

29. Smith III J. (2010), Spherical waves from a point source, [in:] *Physical Audio Signal Processing for Virtual Musical Instruments and Audio Effects*, online version, https://ccrma.stanford.edu/~jos/pasp/Spherical_Waves_Point_Source.html.

30. Staab J., Schady A., Weigand M., Lakes T., Taubenböck H. (2022), Predicting traffic noise using land-use regression – A scalable approach, *Journal of Exposure Science & Environmental Epidemiology*, **32**: 232–243, doi: 10.1038/s41370-021-00355-z.

31. Steele C. (2001), A critical review of some traffic noise prediction models, *Applied Acoustics*, **62**(3): 271–287, doi: 10.1016/S0003-682X(00)00030-X.

32. Stoilova K., Stoilov T. (1998), Traffic noise and traffic light control, *Transportation Research Part D: Transport and Environment,* **3**(6): 399–417, doi: 10.1016/S1361-9209(98)00017-0.

33. Van Renterghem T., Botteldooren D., Verheyen K. (2012), Road traffic noise shielding by vegetation belts of limited depth, *Journal of Sound and Vibration*, **331**(10): 2404–2425, doi: 10.1016/j.jsv.2012.01.006.

34. Yang W., Cai M., Luo P. (2020), The calculation of road traffic noise spectrum based on the noise spectral characteristics of single vehicles, *Applied Acoustics*, **160**: 107128, doi: 10.1016/j.apacoust.2019.107128.

Appendix A. Frequency-dependent road reflection coefficient

The reflection coefficient $C_g(f)$ of the road employed in the model of the current paper takes the averaged values of the measurement data by Li *et al.* (2014) and Knabben *et al.* (2016) for asphalt pavements.

Table 4. Reflection coefficient $C_g(f)$ at 1/3 octave frequencies.

Frequency [Hz]	Reflection coefficient	Frequency [Hz]	Reflection coefficient	Frequency [Hz]	Reflection coefficient
40	0.909	400	0.889	4000	0.689
50	0.908	500	0.883	5000	0.689
63	0.908	630	0.876	6300	0.689
80	0.907	800	0.867	8000	0.689
100	0.906	1000	0.856	10000	0.689
125	0.904	1250	0.842	12500	0.689
160	0.902	1600	0.822	16000	0.689
200	0.900	2000	0.800	20000	0.689
250	0.897	2500	0.772		
315	0.894	3150	0.736		

Appendix B. Vehicle spectral noise database

Based on the noise spectra provided by Yang *et al.* (2020) the authors of this paper have established a vehicle noise database for four vehicle types and five vehicle speed intervals at 28 1/3 octave frequencies.

Table 5. Spectral energy contribution at 1/3 octave frequencies for light vehicle.

Velocity [km/h]	40 Hz	50 Hz	63 Hz	80 Hz	100 Hz	125 Hz	160 Hz	200 Hz	250 Hz	315 Hz
0 ~ 18	0.001	0.005	0.007	0.014	0.019	0.022	0.025	0.045	0.048	0.055
18 ~ 36	0.001	0.005	0.007	0.013	0.019	0.022	0.024	0.044	0.048	0.054
36 ~ 54	0.001	0.005	0.007	0.012	0.018	0.021	0.023	0.043	0.047	0.053
54 ~ 72	0.001	0.004	0.007	0.010	0.017	0.020	0.022	0.043	0.046	0.052
72 ~ 90	0	0.001	0.001	0.001	0.002	0.002	0.005	0.011	0.02	0.013
Velocity [km/h]	400 Hz	500 Hz	630 Hz	800 Hz	1000 Hz	1250 Hz	1600 Hz	2000 Hz	2500 Hz	3150 Hz
0 ~ 18	0.043	0.059	0.084	0.100	0.132	0.089	0.084	0.070	0.046	0.020
18 ~ 36	0.043	0.058	0.083	0.098	0.131	0.090	0.085	0.071	0.047	0.021
36 ~ 54	0.042	0.057	0.082	0.098	0.130	0.091	0.086	0.072	0.048	0.022
54 ~ 72	0.041	0.056	0.082	0.096	0.128	0.093	0.87	0.073	0.049	0.023
72 ~ 90	0.019	0.064	0.06	0.065	0.137	0.152	0.166	0.142	0.078	0.033
Velocity [km/h]	4000 Hz	5000 Hz	6300 Hz	8000 Hz	10000 Hz	12500 Hz	16000 Hz	20000 Hz		
0 ~ 18	0.008	0.004	0.004	0.005	0.003	0.003	0.003	0.002		
18 ~ 36	0.019	0.006	0.005	0.005	0.003	0.003	0.003	0.002		
36 ~ 54	0.011	0.007	0.006	0.006	0.004	0.003	0.003	0.002		
54 ~ 72	0.012	0.009	0.007	0.008	0.004	0.003	0.003	0.002		
72 ~ 90	0.013	0.008	0.004	0.002	0.001	0	0	0		

Table 6. Spectral energy contribution at 1/3 octave frequencies for a medium vehicle.

Velocity [km/h]	40 Hz	50 Hz	63 Hz	80 Hz	100 Hz	125 Hz	160 Hz	200 Hz	250 Hz	315 Hz
0 ~ 18	0.001	0.006	0.015	0.003	0.006	0.011	0.014	0.032	0.046	0.05
18 ~ 36	0.001	0.006	0.014	0.002	0.005	0.009	0.009	0.027	0.042	0.043
36 ~ 54	0.001	0.006	0.012	0.002	0.005	0.008	0.008	0.026	0.037	0.041
54 ~ 72	0.001	0.004	0.01	0.002	0.005	0.008	0.008	0.023	0.034	0.037
72 ~ 90	0.001	0.003	0.005	0.002	0.005	0.007	0.008	0.02	0.034	0.04
Velocity [km/h]	400 Hz	500 Hz	630 Hz	800 Hz	1000 Hz	1250 Hz	1600 Hz	2000 Hz	2500 Hz	3150 Hz
0 ~ 18	0.072	0.091	0.08	0.078	0.067	0.071	0.088	0.077	0.076	0.052
18 ~ 36	0.073	0.096	0.086	0.081	0.067	0.072	0.092	0.077	0.077	0.054
36 ~ 54	0.07	0.09	0.086	0.81	0.07	0.079	0.096	0.081	0.078	0.054
54 ~ 72	0.066	0.086	0.084	0.083	0.074	0.081	0.1	0.084	0.08	0.056
72 ~ 90	0.064	0.08	0.081	0.084	0.079	0.087	0.103	0.086	0.082	0.059
Velocity [km/h]	4000 Hz	5000 Hz	6300 Hz	8000 Hz	10000 Hz	12500 Hz	16000 Hz	20000 Hz		
0 ~ 18	0.029	0.021	0.008	0.004	0.001	0.001	0	0		
18 ~ 36	0.03	0.022	0.009	0.004	0.001	0.001	0	0		
36 ~ 54	0.032	0.022	0.009	0.004	0.001	0.001	0	0		
54 ~ 72	0.034	0.024	0.01	0.004	0.001	0.001	0	0		
72 ~ 90	0.038	0.019	0.008	0.003	0.001	0.001	0	0		

Table 7. Spectral energy contribution at 1/3 octave frequencies for a heavy vehicle.

Velocity [km/h]	40 Hz	50 Hz	63 Hz	80 Hz	100 Hz	125 Hz	160 Hz	200 Hz	250 Hz	315 Hz
0 ~ 18	0	0.001	0.01	0.028	0.011	0.011	0.02	0.04	0.054	0.071
18 ~ 36	0	0.001	0.01	0.026	0.008	0.009	0.017	0.036	0.05	0.068
36 ~ 54	0	0.001	0.01	0.026	0.007	0.008	0.015	0.033	0.047	0.066
54 ~ 72	0	0.001	0.008	0.022	0.006	0.007	0.014	0.031	0.045	0.064
72 ~ 90	0	0.001	0.006	0.02	0.005	0.006	0..013	0.03	0.043	0.06
Velocity [km/h]	400 Hz	500 Hz	630 Hz	800 Hz	1000 Hz	1250 Hz	1600 Hz	2000 Hz	2500 Hz	3150 Hz
0 ~ 18	0.076	0.079	0.073	0.067	0.072	0.071	0.075	0.071	0.064	0.04
18 ~ 36	0.073	0.078	0.073	0.069	0.074	0.074	0.078	0.073	0.067	0.041
36 ~ 54	0.07	0.075	0.074	0.074	0.079	0.077	0.079	0.074	0.068	0.045
54 ~ 72	0.068	0.072	0.071	0.075	0.085	0.081	0.084	0.077	0.071	0.048
72 ~ 90	0.065	0.07	0.071	0.079	0.089	0.086	0.09	0.08	0.073	0.05
Velocity [km/h]	4000 Hz	5000 Hz	6300 Hz	8000 Hz	10000 Hz	12500 Hz	16000 Hz	20000 Hz		
0 ~ 18	0.028	0.017	0.01	0.006	0.003	0.001	0.001	0		
18 ~ 36	0.03	0.019	0.012	0.007	0.004	0.002	0.001	0		
36 ~ 54	0.031	0.018	0.011	0.006	0.003	0.002	0.001	0		
54 ~ 72	0.033	0.018	0.01	0.005	0.002	0.001	0.001	0		
72 ~ 90	0.031	0.016	0.008	0.004	0.002	0.001	0.001	0		

Table 8. Spectral energy contribution at 1/3 octave frequencies for a bus.

Velocity [km/h]	40 Hz	50 Hz	63 Hz	80 Hz	100 Hz	125 Hz	160 Hz	200 Hz	250 Hz	315 Hz
0 ~ 18	0	0.006	0.091	0.101	0.082	0.069	0.075	0.026	0.027	0.031
18 ~ 36	0	0.004	0.088	0.099	0.08	0.067	0.075	0.025	0.025	0.03
36 ~ 54	0	0.004	0.086	0.095	0.077	0.065	0.072	0.025	0.026	0.031
54 ~ 72	0	0.004	0.083	0.092	0.075	0.063	0.069	0.024	0.027	0.032
72 ~ 90	0	0.004	0.08	0.088	0.072	0.06	0.065	0.024	0.028	0.033
Velocity [km/h]	400 Hz	500 Hz	630 Hz	800 Hz	1000 Hz	1250 Hz	1600 Hz	2000 Hz	2500 Hz	3150 Hz
0 ~ 18	0.038	0.037	0.045	0.043	0.041	0.042	0.042	0.044	0.049	0.036
18 ~ 36	0.039	0.038	0.046	0.044	0.042	0.043	0.043	0.045	0.05	0.037
36 ~ 54	0.041	0.04	0.047	0.045	0.043	0.044	0.044	0.046	0.051	0.038
54 ~ 72	0.043	0.042	0.049	0.047	0.044	0.045	0.046	0.048	0.052	0.04
72 ~ 90	0.045	0.044	0.051	0.048	0.046	0.047	0.047	0.049	0.054	0.042
Velocity [km/h]	4000 Hz	5000 Hz	6300 Hz	8000 Hz	10000 Hz	12500 Hz	16000 Hz	20000 Hz		
0 ~ 18	0.029	0.022	0.011	0.008	0.003	0.001	0.001	0		
18 ~ 36	0.031	0.024	0.013	0.007	0.003	0.001	0.001	0		
36 ~ 54	0.032	0.025	0.012	0.006	0.003	0.001	0.001	0		
54 ~ 72	0.033	0.023	0.011	0.005	0.002	0.001	0	0		
72 ~ 90	0.035	0.022	0.01	0.004	0.001	0.001	0	0		

Appendix C. Frequency-dependent sound attenuation by vegetation

The amount of sound attenuation (in dB) by vegetation in the current paper takes the averaged values of the measurement data by Price *et al.* (1988).

Table 9. Sound attenuation by vegetation.

Frequency [Hz]	Amount of sound attenuation [dB]	Frequency [Hz]	Amount of sound attenuation [dB]	Frequency [Hz]	Amount of sound attenuation [dB]
40	2.000	400	2.000	4000	4.000
50	2.000	500	2.000	5000	4.667
63	2.000	630	2.000	6300	5.533
80	2.000	800	2.000	8000	6.667
100	2.000	1000	2.000	10000	8.000
125	2.000	1250	2.167	12500	9.667
160	2.000	1600	2.400	16000	12.000
200	2.000	2000	2.667	20000	14.667
250	2.000	2500	3.000		
315	2.000	3150	3.433		